Landolt-Börnstein

Numerical Data and Functional Relationships
in Science and Technology

Zahlenwerte und Funktionen
aus Naturwissenschaften und Technik

New Series / Neue Serie

Group III

Volume 13

Metals: Phonon States, Electron States and Fermi Surfaces

Subvolume b

Phonon States of Alloys · Electron States
and Fermi Surfaces of Strained Elements

Springer-Verlag
Berlin · Heidelberg · New York

LANDOLT-BÖRNSTEIN

Zahlenwerte und Funktionen
aus Naturwissenschaften und Technik

Neue Serie

Gesamtherausgabe: K.-H. Hellwege

Gruppe III: Kristall- und Festkörperphysik

Band 13

Metalle: Phononenzustände, Elektronenzustände und Fermiflächen

Teilband b

Phononenzustände von Legierungen · Elektronenzustände und Fermiflächen von verformten Elementen

E. Fawcett · R. Griessen · W. Joss · W. Kress

Herausgeber: K.-H. Hellwege und J. L. Olsen

Springer-Verlag Berlin · Heidelberg · New York 1983

CIP-Kurztitelaufnahme der Deutschen Bibliothek

Zahlenwerte und Funktionen aus Naturwissenschaften und Technik/Landolt-Börnstein. – Berlin; Heidelberg; New York: Springer
Parallelt.: Numerical data and functional relationships in science and technology

NE: Landolt, Hans [Begr.]; PT N.S./Gesamthrsg.: K.-H. Hellwege. Gruppe 3, Kristall- und Festkörperphysik. Bd. 13. Metalle: Phononenzustände, Elektronenzustände und Fermiflächen. Teilbd. b. Phononenzustände von Legierungen, Elektronenzustände und Fermiflächen von verformten Elementen/E. Fawcett ··· Hrsg.: K.-H. Hellwege u. J.L. Olsen. – 1983.

ISBN 3-540-10661-8 (Berlin, Heidelberg, New York)
ISBN 0-387-10661-8 (New York, Heidelberg, Berlin)

NE: Hellwege, Karl-Heinz [Hrsg.]; Fawcett, E. [Mitverf.]

Printed in Germany

Typesetting, printing and bookbinding: Universitätsdruckerei H. Stürtz AG Würzburg

2163/3020 - 543210

Table of conversion factors

Quantity	atomic units*)	CGS	SIU	Miscellaneous units
Length, l	$1\,\text{a.u.} = a_0 =$	$5.291772 \cdot 10^{-9}$ cm =	$5.291772 \cdot 10^{-11}$ m =	0.5291772 Å
Energy, E	$1\,\text{a.u.} = \hbar^2/m_{e0}a_0^2 =$	$4.35982 \cdot 10^{-11}$ erg =	$4.35982 \cdot 10^{-18}$ J =	2 Ry (Rydberg) = 27.2116 eV**)
Reciprocal length, l^{-1}	$1\,\text{a.u.} = a_0^{-1} =$	$1.8897 \cdot 10^{8}$ cm^{-1} =	$1.8897 \cdot 10^{10}$ m^{-1} =	1.8897 Å^{-1}
Reciprocal area, A	$1\,\text{a.u.} = a_0^{-2} =$	$3.5711 \cdot 10^{16}$ cm^{-2} =	$3.5711 \cdot 10^{20}$ m^{-2} =	3.5711 Å^{-2}

*) a_0: Bohr radius; m_{e0}: electron rest mass
**) 1 VAs = 1 J = 10^7 erg = $6.24115 \cdot 10^{18}$ eV = $2.3006 \cdot 10^{-4}$ kcal

Conversion factors between Fermi cross section area A and de Haas van Alphen effect frequencies F:
$A = (2\pi e/\hbar)(1/\Delta(1/B))$ with $1/\Delta(1/B) = F$; (all values in SIU)

A in [m^{-2}] $= 9.54575 \cdot 10^{15} \cdot F$ in [T]; $(1\,\text{T} \triangleq 10^4\,\text{G})$;
A in [cm^{-2}] $= 9.54575 \cdot 10^{11} \cdot F$ in [T];
A in [Å^{-2}] $= 9.54575 \cdot 10^{-5} \cdot F$ in [T];
A in [a.u.] $= 2.6731 \cdot 10^{-5} \cdot F$ in [T]

Energy and equivalent quantities

Quantity:		E	$U = E/e$	$\nu = E/h$	$\tilde{\nu} = E/hc$
Unit:		J	V	Hz, s^{-1}	cm^{-1}
1 J	≙	1	$6.24115 \cdot 10^{18}$	$1.50916 \cdot 10^{33}$	$5.03403 \cdot 10^{22}$
1 V	≙	$1.60219 \cdot 10^{-19}$	1	$2.41797 \cdot 10^{14}$	$8.06547 \cdot 10^{3}$
1 s^{-1} = 1 Hz	≙	$6.62619 \cdot 10^{-34}$	$4.13550 \cdot 10^{-15}$	1	$3.33564 \cdot 10^{-11}$
1 cm^{-1}	≙	$1.98648 \cdot 10^{-23}$	$1.23979 \cdot 10^{-4}$	$2.99792 \cdot 10^{10}$	1

Error notation

(xy) applies to the last digits of the value: e.g.

3.478 (21) Å = (3.478 ± 0.021) Å
13.4 (21) Å = (13.4 ± 2.1) Å
9.0 (2) TPa^{-1} = (9.0 ± 0.2) TPa^{-1}
9.0 (25) TPa^{-1} = (9.0 ± 2.5) TPa^{-1}

Survey

Phonon states

Phonon dispersion, frequency spectra and related properties
of metallic elements . . . . . subvolume 13a
of metallic compounds and disordered alloys . . . . . **subvolume 13b**

Electron states and Fermi surfaces

Band structures and Fermi surfaces
of metallic elements . . . . . subvolume 13c
of metallic compounds and disordered alloys . . . . . subvolume 13a
of homogeneously strained metallic elements . . . . . subvolume 13b

Appendix

Unit cells and first Brillouin zones . . . . . subvolume 13a

Übersicht

Phononenzustände

Dispersionskurven, Frequenzspektren und verwandte Eigenschaften
von metallischen Elementen . . . . . Teilband 13a
von metallischen Verbindungen und ungeordneten Legierungen . . . . . **Teilband 13b**

Elektronenzustände und Fermiflächen

Bandstrukturen und Fermiflächen
von metallischen Elementen . . . . . Teilband 13c
von metallischen Verbindungen und ungeordneten Legierungen . . . . . Teilband 13a
von homogen verformten metallischen Elementen . . . . . **Teilband 13b**

Anhang

Einheitszellen und erste Brillouinzonen . . . . . Teilband 13a

Vorwort

Diese Zusammenstellung von Tabellen und Diagrammen ist ein Beitrag zu einem größeren Programm, das eine vollständige und kritische Sammlung der zuverlässigen Daten aus der Metallphysik anstrebt. Da eine vollständige derartige Zusammenstellung noch nicht existiert, sollen diese Daten einem echten Bedürfnis sowohl von Experimentatoren wie von Theoretikern entgegenkommen.

Die Gruppe III in der Neuen Serie des Landolt-Börnstein-Tabellenwerkes ist der Kristall- und Festkörper-Physik gewidmet. Der Band III/13, zu dem der hier vorgelegte Teilband 13b gehört, wird alle bis 1981 publizierten Ergebnisse über Phononen- und Elektronenzustände und Fermiflächen in Metallen berücksichtigen. Sowohl experimentell wie auch theoretisch gewonnene Daten sind aufgenommen.

Um die Publikation zu beschleunigen, werden die Beiträge der verschiedenen Autoren in drei Teilbänden 13a, 13b, 13c zum Druck gegeben, sobald die Manuskripte fertiggestellt sind. Die Tabellen erscheinen somit in chronologischer statt in thematischer Reihenfolge. Eine systematische Übersicht ist im vorderen Buchdeckel abgedruckt.

Dieser Teilband enthält zwei Daten-Sammlungen: eine von Phononenzuständen in Verbindungen und Legierungen, und die andere von Elektronenzuständen und Fermiflächen von homogen verformten Elementen.

Im allgemeinen wird die in der Literatur gebräuchliche Nomenklatur einschließlich der Symbole auch in den Tabellen verwendet; wegen Einzelheiten sei der Leser auf die Einführungen zu den verschiedenen Beiträgen verwiesen.

Unser besonderer Dank gilt den Autoren, die sich der äußerst mühevollen Aufgabe unterzogen haben, die Daten für diesen Teilband zu sammeln und in Tabellen und Abbildungen kritisch aufzuarbeiten. Wir sind überzeugt, daß ihr Beitrag von hohem Wert für die Physik sein wird, und wir hoffen, daß die Autoren hierin Lohn für ihre harte und sorgfältige Arbeit finden werden.

Unser Dank gilt auch der Landolt-Börnstein-Redaktion, insbesondere Herrn Dr. H. Seemüller für die redaktionelle Betreuung dieses Teilbandes, sowie Frau D. Dolle, Frau R. Lettmann und Frau R. Schattschneider für die sorgfältige Überprüfung der Manuskripte und Druckfahnen.

Dem Springer-Verlag danken wir für die verständnisvolle Zusammenarbeit bei der Fertigstellung.

Wie alle anderen Landolt-Börnstein-Bände wird auch dieser Teilband ohne Zuschüsse von anderer Seite publiziert.

Darmstadt und Zürich, Dezember 1982 **Die Herausgeber**

Preface

This collection of tables and diagrams is a contribution to a larger programme aiming at a complete and critical tabulation of reliable data relevant to metal physics. No such complete collection exists at present, and these tables should fill a long felt need of both experimentalists and theoreticians.

Group III in the New Series of the Landolt-Börnstein tables deals with Crystal and Solid State Physics. Volume III/13, to which this subvolume 13b belongs, will cover all data published up to 1981 on phonon and electron states and Fermi surfaces in metals. Both experimental and theoretical results are included.

To hasten publication the compilations in the subvolumes 13a, 13b, and 13c are being printed after each author has completed his manuscript. The order of the tables is thus chronological rather than thematic. A systematic survey is given on the inside of the cover.

This subvolume contains two data compilations, one of phonon states of metallic compounds and disordered alloys, and the other of electron states and Fermi surfaces of homogeneously strained metallic elements.

In general, symbols and nomenclature are those used in the literature but the reader is referred to the separate contributions for detailed information.

Our most grateful thanks are due to the authors for taking on the very laborious task of collecting the data and critically preparing the tables in this subvolume. We are confident that their contribution will be of great value to the physics community, and we hope that the authors will find in this a reward for all their hard and careful work.

Thanks are also due to the editorial staff of Landolt-Börnstein, especially to Dr. H. Seemüller who was in charge of the editorial preparation of this subvolume, and to Frau D. Dolle, Frau R. Lettmann and Frau R. Schattschneider, for their careful checking of the manuscripts and galleys.

We are also grateful to the Springer-Verlag for their patient care and experienced help in the final preparation.

As in the case of other Landolt-Börnstein volumes, this subvolume is published without outside financial support.

Darmstadt and Zürich, December 1982 **The Editors**

Contents

3 Electron states and Fermi surfaces of homogeneously strained metallic elements

W. Joss*†), Laboratorium für Festkörperphysik, Eidgenössische Technische Hochschule Zürich, 8093 Zürich, Switzerland

R. Griessen, Natuurkundig Laboratorium der Vrije Universiteit, Amsterdam, The Netherlands

E. Fawcett, Department of Physics, University of Toronto, Toronto, Canada

3.1 Introduction 1

3.1.1 General remarks 1
3.1.2 Presentation of the Selected data in section 3.3 1
3.1.3 Experimental methods and their abbreviations 2
3.1.4 Abbreviations of theoretical methods 3
3.1.5 List of frequently used symbols and abbreviations 4
3.1.6 Definition of stresses, strains, angular and tetragonal shears 6
3.1.7 Relations between hydrostatic pressure, stress and strain derivatives of extremal cross-sectional areas of the Fermi surface 7
3.1.8 Predictions of simple models 8
3.1.9 General references for 3.1 9

3.2 Literature survey of calculations and experiments on electron states and Fermi surfaces of homogeneously strained metallic elements 11

3.3 Data 16

Ag 16
Al 20
Am 34
As 35
Au 37
Ba 40
Be 41
Bi 46
C 56
Ca 60
Cd 69
Ce 74
Co 75
Cr 76
Cs 87
Cu 97
Fe 104
Ga 108
Gd 111
Hg 113
In 114
Ir 118
K 119
La 122
Li 127
Mg 129
Mo 134
Na 146
Nb 148
Ni 152
Np 156
Os 157
Pa 158
Pb 158
Pd 172
Pt 180
Pu 180
Rb 181
Re 183
Rh 188
Ru 189
Sb 193
Sn 201
Sr 210
Tc 212
Th 213
Ti 215
Tl 216
U 219
V 221
W 226
Y 234
Yb 235
Zn 236
Zr 247

3.4 References for 3.2 and 3.3 248

*) Work supported in part by the Schweizerischer Nationalfonds zur Förderung der wissenschaftlichen Forschung.

†) Present address: Solid State Science Division, Argonne National Laboratory, Argonne, Illinois 60439.

4 Phonon dispersion, one-phonon density of states and impurity vibrations in metallic compounds and disordered alloys

W. KRESS, Max Planck Institut für Festkörperforschung, Stuttgart Germany

4.1 Introduction . . . 259
4.1.1 General remarks . . . 259
4.1.2 Theory of lattice vibrations . . . 260
4.1.3 Inelastic neutron scattering by phonons . . . 264
4.1.4 Refractory compounds . . . 267
4.1.5 Mixed valent compounds . . . 268
4.1.6 Layered compounds . . . 269
4.1.7 Linear conductors . . . 269
4.1.8 Hydrogen in metals . . . 271
4.1.9 Impurities . . . 272
4.1.10 List of frequently used symbols and abbreviations, table of energy conversion factors . . . 273
4.1.11 Survey of the compounds compiled in section 4.2 . . . 274
4.1.12 Alphabetical index of the compounds compiled in section 4.2 . . . 276

4.2 Data . . . 281
4.2.1 NaCl(B1)-structure compounds . . . 281
4.2.1.1 Group IVb refractory compounds . . . 281
4.2.1.2 Group Vb refractory compounds . . . 285
4.2.1.3 Y- and rare earth compounds . . . 290
4.2.1.4 Actinide compounds . . . 294
4.2.2 $Cu_3Au(L1_2)$-structure compounds . . . 299
4.2.3 Bronzes . . . 306
4.2.4 Laves phases . . . 308
4.2.5 Chevrel phases . . . 310
4.2.6 Miscellaneous . . . 312
4.2.7 Layered metallic compounds . . . 317
4.2.8 Linear conductors . . . 320
4.2.8.1 A15 compounds . . . 320
4.2.8.2 Other compounds . . . 325
4.2.9 Hydrogen in metals . . . 333
4.2.10 Disordered alloys (solid solutions) . . . 355
4.2.10.1 Defects . . . 355
4.2.10.2 fcc host lattices . . . 357
4.2.10.3 Invar alloys . . . 375
4.2.10.4 bcc host lattices . . . 380
4.2.10.5 hcp and other host lattices . . . 391
4.2.10.6 Miscellaneous . . . 394

4.3 References for 4.1 and 4.2 . . . 396

3 Electron states and Fermi surfaces of homogeneously strained metallic elements

3.1 Introduction

3.1.1 General remarks

Since the first measurements of the hydrostatic pressure dependence of extremal cross-sectional areas of the Fermi surface of bismuth by Verkin, Dmitrenko and Lazarev in 1956 [56v1], a considerable amount of work has been done to determine the stress and strain dependence of the Fermi surface of metallic elements. In parallel to this experimental activity theorists developed powerful methods to calculate the volume and the strain dependence of electronic band structures, electronic densities of states and Fermi surfaces.

The purpose of this part of the tables is to present up-to-date data on nonlocalized single-particle electronic states in homogeneously strained metallic elements. These data are directly related to important properties of metals such as ultrasonic attenuation and thermal expansion at low temperatures, elastic moduli, cohesive energy, electron-phonon interaction, and to the pressure, stress and strain dependence of the superconducting transition temperature, the electronic specific heat and the Pauli spin susceptibility. Information on the relation between the strain dependence of the electronic structure of a metal and the physical properties mentioned above may be found in the review articles [71b1, 74s1, 74s2, 80b2, 80f1, 80i1] and in standard solid state physics books [70h1, 70h2, 70h3, 72z1, 76a1].

The tables are organized as follows: In the Literature survey given in section 3.2, we have included all the published data related to the strain and/or stress dependence of the electronic structure of metals contained in Physics Abstracts until the end of 1980. In this survey references are given chronologically without any consideration for accuracy or reliability of the published results. In section 3.3, however, we give information on the strain and/or stress dependence of the electronic structure of metallic elements obtained from a critical selection of the works indicated in the Literature survey of section 3.2. A detailed description of the presentation of the information of the Selected data is given in section 3.1.2. The references mentioned in the Literature survey and in the Selected data (section 3.3) are given in section 3.4.

3.1.2 Presentation of the selected data in section 3.3

In order to facilitate access to the data, the metallic elements are classified alphabetically according to their chemical symbol from Ag to Zr. For each element we give the following specific information under the headings:

Element

The crystal structure(s) and lattice parameter(s). The lattice parameter(s) a_0 at 0 K is (are) determined from room temperature X-ray measurements [67p1, 71e1] and thermal expansion data [76t1], if not indicated otherwise. The low temperature lattice spacing is indicated since most of the experimental work has been carried out at liquid helium temperatures.

A reference for the Brillouin zone corresponding to the crystal structure of the element.

Fermi surface

A schematic three-dimensional picture of the currently accepted Fermi surface together with representative extremal cross-sections for a proper identification of the extremal orbits observed in quantum oscillatory effects. If necessary, cross-sections of the Fermi surface in high symmetry planes are also indicated.

Stress and strain dependence of the Fermi surface

a) Tables with *hydrostatic pressure* ($\mathrm{d} \ln A/\mathrm{d}p$), *uniaxial stress* ($\mathrm{d} \ln A/\mathrm{d}\sigma_i$), *uniaxial strain* ($\mathrm{d} \ln A/\mathrm{d}\varepsilon_i$), *tetragonal shear* ($\mathrm{d} \ln A/\mathrm{d}\gamma_i$) and *angular shear* ($\mathrm{d} \ln A/\mathrm{d}\gamma_{ij}$) derivatives of extremal cross-sectional areas A of the Fermi surface.

In all tables the orbit corresponding to a given extremal cross-section of the Fermi surface is identified by:

the symbol ($\Psi, \alpha, \beta, \ldots$), the name (waist, belly, neck, ...) currently used to designate the orbit and/or the name (cigar, needle, monster, jungle-gym) of the Fermi surface sheet it belongs to.

the type ("electron-like" or "hole-like") of the orbit and the number of the band it belongs to (h_2 is, for example, a hole-like orbit in the second band and e_3, an electron-like orbit in the third band).

the position of its centre specified by means of an appropriate symbol if it is a high-symmetry point of the Brillouin zone, the k_x, k_y, k_z coordinates or a symmetry direction in reciprocal space.

the direction of the normal $\boldsymbol{n}$ to the plane of the orbit (in experiments such as de Haas-van Alphen, Schubnikov-de Haas, oscillatory magnetostriction, sound velocity and ultrasonic attenuation, the direction of the applied magnetic field is parallel to that of the vector $\boldsymbol{n}$).

an approximate value of the de Haas-van Alphen frequency F and the corresponding extremal area A.

Pressure derivatives $\mathrm{d}\ln A/\mathrm{d}p$ are usually determined from hydrostatic pressure measurements. In some cases $\mathrm{d}\ln A/\mathrm{d}p$ has been derived from uniaxial stress or strain derivatives by means of Eqs. (9) or (14) in section 3.1.7. For comparison with theoretical calculations the hydrostatic pressure derivatives $\mathrm{d}\ln A/\mathrm{d}p$ are converted to volume derivatives $\mathrm{d}\ln A/\mathrm{d}\ln\Omega$ by means of Eq. (8) in section 3.1.7. Similarly the uniaxial stress derivatives $\mathrm{d}\ln A/\mathrm{d}\sigma_i$ are usually determined from measurements of quantum oscillatory effects under direct stress or of oscillatory magnetostriction. In some cases $\mathrm{d}\ln A/\mathrm{d}\sigma_i$ has been calculated from experimental strain derivatives by means of Eq. (10) in section 3.1.7. For these conversions or for any other conversion with one of the equations given in 3.1.7 we used the elastic moduli at 0 K given in [79h1] if not specified otherwise.

b) Figures of the local distortion produced by a homogeneous strain on various cross-sections of the Fermi surface as obtained from parametrization schemes or first principles calculations.

c) Figures giving the strain or stress derivatives of extremal cross-sectional areas of the Fermi surface as a function of the crystal orientation.

d) If available, extra experimental information such as extremal Fermi surface areas or de Haas-van Alphen frequencies as function of pressure, influence of the pressure medium, volume dependence of the Fermi wave vector as determined from positron annihilation experiments under hydrostatic pressure.

Theoretical models

a) *Parametrization schemes* based on the OPW, TB-NFE or KKR methods of band structure calculations used to invert de Haas-van Alphen data (extremal cross-sections of the Fermi surface) to $\boldsymbol{k}$-point data in reciprocal space. In tables we indicate the value of the fitting parameters used to invert the data given in the section Stress and strain dependence of the Fermi surface.

For the orthogonalized-plane-wave OPW-parametrization schemes the relevant parameters are the Fermi energy E_F, the pseudopotential matrix elements $v_s = v(|\boldsymbol{G}_s|)$ and their volume derivatives, $\mathrm{d}\ln E_F/\mathrm{d}\ln\Omega$ and $\mathrm{d}\ln v_s/\mathrm{d}\ln\Omega$. As $\mathrm{d}\ln v_s/\mathrm{d}\ln\Omega$ is essentially determined by the slope $(\partial v/\partial \ln q)_{q=|\boldsymbol{G}_s|}$ of the form factor $v(q)$ at the reciprocal lattice vector $\boldsymbol{G}_s$, we include this quantity in the table and compare it to theoretical models in a figure of the pseudopotential form factor [81j1].

For the hybrid tight-binding nearly-free-electron TB-NFE parametrization schemes the relevant parameters are the d-resonance width Γ, the resonance position E_d, the overlap integrals $dd\chi$ ($\chi = \sigma, \pi, \delta$), the Fermi energy E_F, the plane wave matrix elements, and their volume and strain derivatives [75p1].

For the parametrization schemes based on the Kohn-Korringa-Rostoker KKR band structure model the tabulated parameters are the Fermi energy E_F, the s, p, d ($l = 0, 1, 2$) phase-shifts η_l (in the relativistic case $\eta_{l,j}$) and their volume derivatives $\mathrm{d}\eta_l/\mathrm{d}\ln\Omega$ [77g2]. A peculiar feature of the KKR-parametrization scheme is that the value of E_F and $\mathrm{d}\ln E_F/\mathrm{d}\ln\Omega$ can be arbitrarily chosen within a reasonable range of values [80b1].

For other parametrization schemes such as the various Fourier expansion FF-schemes the tabulated coefficients are either defined in a footnote of the table or reference is made to the original article.

b) The results of *first principles calculations* on the strain dependence of energy levels, band widths and partial electron charges inside and outside the muffin-tin spheres are indicated in tables while energy band electron density of states and radial wave functions for various homogeneous deformations of the lattice are given in figures.

3.1.3 Experimental methods and their abbreviations

Information on the dimensions of the Fermi surface of a metal is obtained from measurements of:

DHVA	the de Haas-van Alphen effect [55l1, 68g1, 68s3, 68w1]
GM	galvanomagnetic effects [73l1]
M	oscillatory magnetization [68g1, 71t1]
OGM	oscillatory galvanomagnetic effects [70r2, 73l1]
OM	oscillatory magnetostriction [71c1]
OS	optical spectroscopy
OTM	oscillatory thermomagnetic effects [66c1, 73l1]

PA	positron annihilation
SDH	the Shubnikov-de Haas effect [73l1]
SV	quantum oscillations in sound velocity [71t1]
T	the de Haas-van Alphen torque [64c1, 68g1, 73g1]
TM	thermomagnetic effects [73l1]
TP	transport properties [73l1]
UA	ultrasonic attenuation [70r1]

The hydrostatic pressure dependence of extremal cross-sectional areas of the Fermi surface is measured by means of one of the following experimental techniques:

FHe	the fluid helium phase-shift technique in which the phase of a quantum oscillatory signal at a fixed magnetic field is measured as a function of pressure. As a result of their high phases (typically $10^3 - 10^4$) changes in the frequency F of quantum oscillatory effects can already be detected at pressures smaller than 2.5 MPa using liquid helium as pressure medium [66t2].
SHe	the solid helium technique, also called the isobaric freezing technique, in which quantum oscillatory effects such as the de Haas-van Alphen or Schubnikov-de Haas effect are measured as a function of hydrostatic pressure transmitted by helium at pressures between 0.1 and 1 GPa [70s1].
SHe – PS	the solid helium phase-shift technique is essentially the same as FHe, except that the pressure medium is solid helium [76s1].
S – OIL	the pseudo-hydrostatic methods in which transformer oil or mixtures of oil and pentane are used as pressure medium. These methods are otherwise similar to SHe [63i1].
ICE	as SHe but with ice as pressure medium [58d1].

The uniaxial stress dependence of extremal cross-sectional areas of the Fermi surface is measured by means of the following experimental methods [80f1]

DS	the direct stress method in which a uniaxial compression or dilation is applied to a sample in order to induce a change in the frequency of quantum oscillatory effects [72s2].
OM	the oscillatory magnetostriction method. This method can only be used for metals with a well known Fermi surface as it requires accurate values for all the parameters (effective mass, Dingle temperature, g-factor, etc.) which enter the theoretical Lifshitz-Kosevich [55l1] relation for the free energy of an electron gas in a magnetic field [72a1].
OM + M	the combined method in which the amplitudes of oscillatory magnetostriction and magnetization are measured simultaneously as a function of magnetic field [77s1].
OM + T	the combined method in which the amplitude of the oscillatory magnetostriction and the de Haas-van Alphen torque are measured simultaneously as a function of magnetic field [77g2, 81j1].

Furthermore the magnitude (but not the actual sign) of the uniaxial strain dependence of extremal cross-sectional areas of the Fermi surface may be measured by means of the following combined methods:

SV + M	in this method the amplitudes of quantum oscillations in the sound velocity and in the magnetization are measured simultaneously as a function of magnetic field [71t1].
SV + T	this method is the same as SV + M except that the amplitude of the de Haas-van Alphen torque is used instead of that of the oscillatory magnetization [77s1].

3.1.4 Abbreviations of theoretical methods

In this section we give only the names of the methods used in electron band structure calculations. Description of these methods may be found in the references indicated hereafter or in [69h2, 70h1, 71z1, 76a1]. For applications to the case of homogeneously strained metals see also Theoretical models in section 3.1.2.

AOPW	approximate analytical OPW-method [79w1]
APW	augmented-plane wave method [37s1, 67l1, 68m1, 71d1]
ASA	atomic-sphere-approximation [80m1]
CEL	cellular method [65a1, 68a1]
FF	Fourier-series expansion method [69h1, 70b1]
HUB	Hubbard model [68h1, 72h1]
KKR	Green's functions or Korringa-Kohn-Rostoker method [47k1, 54k1, 61h1, 68s1, 71d1]
KKRPS	phase-shift parametrization scheme based on the KKR method [72s1, 75k1]
KP	$\boldsymbol{k} \cdot \boldsymbol{p}$-method [66k1]

LAPW	linearized APW method [75k2]
LCAO	linear combination of atomic orbitals method [54s1]
LMTO	linear combination of muffin-tin orbitals method [75a1, 80m1]
NFE	nearly-free-electron model
OPW	orthogonalized plane wave method [66h1, 68s2, 70c1, 70h2, 70h3]
PT	perturbation theory [75g1, 76g1]
RAPW	relativistic APW-method [71d1]
RKKR	relativistic KKR-method [66o1, 66t1]
RNA	renormalized atom method [77g1]
ROPW	relativistic OPW-method [63f1, 66w1]
SC–APW	self-consistent APW-method [71d1, 72p1]
SC–CEL	self-consistent CEL-method [72t1]
SC–RAPW	self-consistent RAPW-method
TB	method based on the tight-binding approximation [54s1, 69f1]
TB–NFE	tight-binding nearly-free-electron hybrid model [66h2, 67m1, 69h2, 69p1]

3.1.5 List of frequently used symbols and abbreviations [1])

Symbols

a [Å]	lattice spacing
a_0 [Å]	equilibrium lattice spacing at 0 K
A [a.u.]	area of an extremal cross-section of the Fermi surface
A···Z	high symmetry points in the Brillouin zone
$\boldsymbol{B}$ [T]	magnetic induction
B_s [Ry]	bottom of the conduction band
ΔB [T]	shift of the de Haas-van Alphen oscillations in measurements using the FHe or SHePS phase-shift technique
C_{ij} [Pa]	elastic stiffness modulus (i, j = 1, …, 6) at 0 K
C_j	coefficient of the Fourier series representation of the Fermi surface
C_l [Ry]	energy of the centre of l = s, p, d bands in band structure calculations based on the atomic-sphere-approximation ASA and using linear combinations of muffin-tin orbitals LMTO.
d_0 [Ry]	energy of the centre of the d-band in tight-binding models (TB, TB–NFE)
$dd\chi_i$ [Ry]	i-th nearest-neighbour d–d-overlap integral ($\chi = \sigma$, π or δ)
e_i	electron-like orbit in the i-th energy band
E [Ry]	energy
E_b [Ry]	energy of the bottom of the d-band
E_c [Ry]	cohesive energy
E_{cr} [Ry]	critical Fermi energy for a Lifshitz transition LT
E_d [Ry]	position in energy of the resonance in the l = 2 phase shift η_2
E_F [Ry]	Fermi energy
E_{F0} [Ry]	Fermi energy of a free electron gas
E_t [Ry]	energy of the top of the d-band
F [T]	dc Haas-van Alphen frequency
$\boldsymbol{G}_s$	reciprocal lattice vector in direction s (e.g. s = [010])
h_i	hole-like orbit in the i-th energy band
$\boldsymbol{H}$ [A/m]	magnetic field
$\boldsymbol{k}$ [a.u.] [2])	wave-vector of a Bloch electron state
k_F [a.u.] [2])	Fermi wave vector, $k_F = \lvert\boldsymbol{k}_F\rvert$
k_{F_0} [a.u.] [2])	free-electron Fermi wave vector
m^* [m_e]	renormalized (enhanced) effective electron mass (in units of m_e)
m_b^* [m_e]	band structure effective electron mass (in units of m_e)
m_e [kg]	rest mass of the electron = $9.10956 \cdot 10^{-31}$ kg
$\boldsymbol{n}$	unit vector normal to the plane of an extremal cross-section of the Fermi surface (in dc Haas-van Alphen experiments $\boldsymbol{n}$ is parallel to the magnetic induction $\boldsymbol{B}$)
$n(E)$ $\left[\frac{\text{states}}{\text{atom Ry}}\right]$	total density of states at energy E

$n_l(E)$ $\left[\frac{\text{states}}{\text{atom Ry}}\right]$	partial density of states at E (if $i=l=s, p, d, f$ then $n_l(E)$ is the density of states with a symmetry corresponding to a definite value of the angular quantum number l; if $i=1, 2, 3$ then $n_i(E)$ is the density of states of the i-th energy band)
N $\left[\frac{\text{electrons}}{\text{atom}}\right]$	total number of conduction electrons per atom
N_l $\left[\frac{\text{electrons}}{\text{atom}}\right]$	number of $l=s, p, d$ conduction electrons per atom
p [Pa]	hydrostatic pressure (the corresponding stresses are $\sigma_1=\sigma_2=\sigma_3=-p$)
P [1/T]	period of de Haas-van Alphen oscillations, $P=1/F$
q [a.u.] [2])	difference of two k-vectors, $\|q\|=q$
Q_l [e_0]	electrical charge (in units of the electron charge $e_0=1.60219\cdot10^{-19}$ C) of the states with symmetry $l=s, p, d, f$ inside the muffin-tin sphere
Q_{out} [e_0]	total electrical charge (in units of the electron charge $e_0=1.60219\cdot10^{-19}$ C) outside the muffin-tin sphere
R_i [Å], [a.u.]	distance between a given atom and its i-th nearest neighbour
R_{ws} [a.u.]	Wigner-Seitz radius
S_{ij} [Pa^{-1}]	elastic compliance modulus (i, j=1, ..., 6) at 0 K.
T [Ry]	kinetic energy
T_c [K]	critical temperature of a superconductor
$v(q)$ [Ry]	pseudopotential form factor $v(\|\boldsymbol{G}_s\|)=v(q)\|_{q=\|\boldsymbol{G}_s\|}$
V_{klm} [Ry]	pseudopotential matrix element associated with the reciprocal lattice vector $\boldsymbol{G}_{klm}$
V_i [a.u.]	volume of the i-th Fermi surface sheet
V_{MTZ} [Ry]	energy of the muffin-tin zero
W_d [Ry]	width of the d-band
α	exchange parameter
β	cut-off parameter in the tight-binding nearly-free-electron hybrid model TB – NFE
β'	parameter of the point-ion form factor
γ_i	tetragonal shear (i=x, y, z). For a definition see section 3.1.6
γ_{ij}	angular shear (i, j=x, y, z). For a definition see section 3.1.6
Γ	centre of the Brillouin zone
Γ [Ry]	width of the resonance in the l=2 phase shift η_2
Δ_s	spin-splitting shift in quantum oscillations
ε_i	uniaxial strain (i=1, 2, 3 and 1≡[100], 2≡[010], 3≡[001]). For a definition see section 3.1.6
$\varepsilon(q)$	Lindhard dielectric function
η_l [rad]	non-relativistic scattering phase-shift
$\eta_{l,j}$ [rad]	relativistic scattering phase-shift
κ_T [Pa^{-1}]	isothermal compressibility at 0 K
$\Lambda, \Delta, \Sigma, \ldots$	high symmetry lines in the Brillouin zone
μ_l	band mass of the l-th band in calculations based on the atomic-sphere approximation ASA and using linear combinations of muffin-tin orbitals LMTO
ξ [Ry]	spin-orbit parameter in tight-binding models TB or TB – NFE
ϱ	axial ratio c/a (c is the lattice spacing in the direction of the highest symmetry axis)
σ_i [Pa]	uniaxial stress (i=1, ..., 6 and 1≡[100], 2≡[010], 3≡[001]). For a definition see section 3.1.6
ϕ [rad]	shift in the phase of the de Haas-van Alphen signal in measurements using the FHe or SHePS phase-shift technique
Φ [Ry]	potential energy
Ω [a.u.]	atomic volume
Ω_0 [a.u.]	equilibrium atomic volume
↑	spin-up, majority electrons
↓	spin-down, minority electrons

[1]) See also table of conversion factors.
[2]) In most cases k is normalized to the dimensions of the BZ.

Abbreviations (see also sections 3.1.3 and 3.1.4)

BZ	Brillouin zone
bcc	body-centered-cubic crystal structure
fcc	face-centered-cubic crystal structure
FIT	value fitted to experimental data (see section 3.1.2, theoretical models)
hcp	hexagonal-closed-packed crystal structure
LT	Lifshitz transition (topology change of the Fermi surface) [60l1]
MB	magnetic breakdown [67s1]

3.1.6 Definition of stresses, strains, angular and tetragonal shears

To introduce the notation adopted to describe lattice deformations, consider three orthogonal unit vectors x, y and z attached to the unstrained lattice. Under a small homogeneous deformation of the solid these vectors take the form

$$\begin{aligned} x' &= (1+\varepsilon_{xx})x + \varepsilon_{xy}y + \varepsilon_{xz}z \\ y' &= \varepsilon_{yx}x + (1+\varepsilon_{yy})y + \varepsilon_{yz}z \\ z' &= \varepsilon_{zx}x + \varepsilon_{zy}y + (1+\varepsilon_{zz})z \end{aligned} \tag{1}$$

In this work we use the notation

$$\varepsilon_{xx}=\varepsilon_1, \quad \varepsilon_{yy}=\varepsilon_2, \quad \varepsilon_{zz}=\varepsilon_3, \tag{2}$$

for the *strains* ε_i (i=1, 2, 3) and for cubic crystals

$$\varepsilon_1=\varepsilon_{100}, \quad \varepsilon_2=\varepsilon_{010}, \quad \varepsilon_3=\varepsilon_{001}.$$

For the *angular shears* γ_{ij} (i, j=x, y, z; i≠j) we use

$$\begin{aligned} \gamma_{xy} &= \gamma_{yx} = (\varepsilon_{xy}+\varepsilon_{yx}) \\ \gamma_{yz} &= \gamma_{zy} = (\varepsilon_{yz}+\varepsilon_{zy}) \\ \gamma_{zx} &= \gamma_{xz} = (\varepsilon_{zx}+\varepsilon_{xz}) \end{aligned} \tag{3}$$

The lattice strains ε_i and angular shears γ_{ij} are linear combinations of the lattice stresses σ_i, so that

$$(\varepsilon_1, \varepsilon_2, \varepsilon_3, \gamma_{yz}, \gamma_{zx}, \gamma_{xy}) = \{S_{ij}\}(\sigma_1, \sigma_2, \sigma_3, \sigma_4, \sigma_5, \sigma_6) \tag{4}$$

where $\{S_{ij}\}$ is the 6×6-matrix of elastic compliance moduli. Similarly, the stresses are related to the strains by means of

$$(\sigma_1, \sigma_2, \sigma_3, \sigma_4, \sigma_5, \sigma_6) = \{C_{ij}\}(\varepsilon_1, \varepsilon_2, \varepsilon_3, \gamma_{yz}, \gamma_{zx}, \gamma_{xy}) \tag{5}$$

where $\{C_{ij}\}$ is the 6×6-matrix of elastic stiffness moduli. For cubic crystals we use the notation

$$\sigma_1=\sigma_{100}, \quad \sigma_2=\sigma_{010}, \quad \sigma_3=\sigma_{001}.$$

The relative volume dilation $\Delta\Omega/\Omega$ corresponding to a given lattice strain is given by

$$\frac{\Delta\Omega}{\Omega} = \varepsilon_1+\varepsilon_2+\varepsilon_3. \tag{6}$$

In *cubic crystals* it is advantageous to express the state of strain as a superposition of an isotropic dilation $\Delta\Omega/\Omega$, the three angular shears γ_{ij} given in Eq. (3) and three tetragonal shears γ_i (i=x, y, z).

A tetragonal shear along the z-axis is the following combination of the fractional strains ε_i,

$$\varepsilon_{xx}=\varepsilon_{yy}=-\tfrac{1}{2}\gamma_z \tag{7}$$

and

$$\varepsilon_{zz}=\gamma_z$$

The strains corresponding to the tetragonal shears γ_x and γ_y are simply obtained by cyclic permutation of the indices in Eqs. (7). In the following equations we use also the notation: $\gamma_x=\gamma_1$, $\gamma_y=\gamma_2$ and $\gamma_z=\gamma_3$. Distorsions of a unit cube by an isotropic dilation, a positive tetragonal shear and a positive angular shear in real space are shown in Fig. 1. The corresponding situation in reciprocal space is shown in Fig. 2.

Both the tetragonal and angular shears are volume conserving deformations. These deformations have the interesting property that they leave scalar properties such as the Fermi energy E_F, the volume of a given sheet of the Fermi surface, the bottom of the conduction band, the density of states at E_F and the spherical scattering phase shifts η_l unchanged.

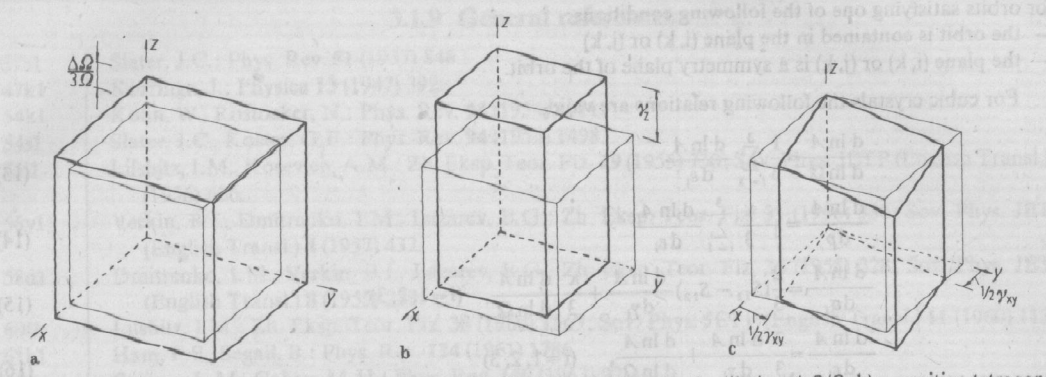

Fig. 1a–c. Distortions (heavy lines) of a unit cube (light lines) by a) an isotropic dilation $\Delta\Omega/\Omega$, b) a positive tetragonal shear γ_z and c) a positive angular shear γ_{xy}.

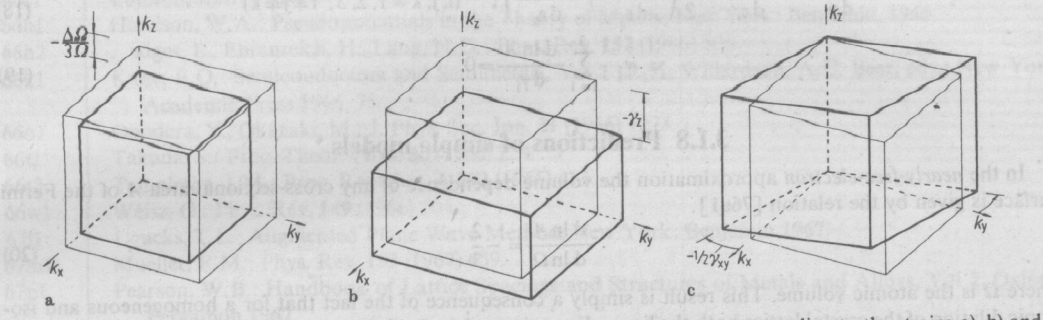

Fig. 2a–c. Distortions (heavy lines) of a unit cube (light lines) in *reciprocal space* corresponding to the strains a), b) and c) in Fig. 1.

3.1.7 Relations between hydrostatic pressure, stress and strain derivatives of extremal cross-sectional areas of the Fermi surface

From the definitions given in section 3.1.6 one can derive the following useful relations for the derivatives of the extremal cross-sectional area A of a given orbit of the Fermi surface,

$$\frac{d \ln A}{dp} = -\kappa \frac{d \ln A}{d \ln \Omega} \tag{8}$$

$$\frac{d \ln A}{dp} = -\sum_{i=1}^{3} \frac{d \ln A}{d\sigma_i} \tag{9}$$

$$\frac{d \ln A}{d\sigma_i} = \sum_{j=1}^{3} S_{ij} \frac{d \ln A}{d\varepsilon_j}, \quad (i=1,2,3) \tag{10}$$

$$\frac{d \ln A}{d\varepsilon_i} = \sum_{j=1}^{3} C_{ij} \frac{d \ln A}{d\sigma_j}, \quad (i=1,2,3) \tag{11}$$

For angular shears one has furthermore,

$$\frac{d \ln A}{d\gamma_{ij}} = 0, \quad (i, j = x, y, z;\ i \neq j) \tag{12}$$

for orbits satisfying one of the following conditions:
- the orbit is contained in the plane (i, k) or (j, k)
- the plane (i, k) or (j, k) is a symmetry plane of the orbit.

For cubic crystals the following relations are valid,

$$\frac{d\ln A}{d\ln\Omega}=\frac{1}{3}\sum_{i=1}^{3}\frac{d\ln A}{d\varepsilon_i} \tag{13}$$

$$\frac{d\ln A}{dp}=-\frac{\kappa}{3}\sum_{i=1}^{3}\frac{d\ln A}{d\varepsilon_i} \tag{14}$$

$$\frac{d\ln A}{d\sigma_i}=\frac{2}{3}(S_{11}-S_{12})\frac{d\ln A}{d\gamma_i}+\frac{\kappa}{3}\frac{d\ln A}{d\ln\Omega}, \quad (i=1,2,3) \tag{15}$$

$$\frac{d\ln A}{d\varepsilon_i}=\frac{2}{3}\frac{d\ln A}{d\gamma_i}+\frac{d\ln A}{d\ln\Omega}, \quad (i=1,2,3) \tag{16}$$

$$\frac{d\ln A}{d\gamma_i}=(C_{11}-C_{12})\left[\frac{d\ln A}{d\sigma_i}-\frac{1}{2}\left(\frac{d\ln A}{d\sigma_j}+\frac{d\ln A}{d\sigma_k}\right)\right], \quad (i,j,k=1,2,3;\ i\neq j\neq k) \tag{17}$$

$$\frac{d\ln A}{d\gamma_i}=\frac{d\ln A}{d\varepsilon_i}-\frac{1}{2}\left(\frac{d\ln A}{d\varepsilon_j}+\frac{d\ln A}{d\varepsilon_k}\right), \quad (i,j,k=1,2,3;\ i\neq j\neq k) \tag{18}$$

$$\sum_{i=1}^{3}\frac{d\ln A}{d\gamma_i}=0. \tag{19}$$

3.1.8 Predictions of simple models

In the *nearly-free-electron* approximation the volume dependence of any cross-sectional area A of the Fermi surface is given by the relation [76a1]

$$\frac{d\ln A}{d\ln\Omega}=-\frac{2}{3} \tag{20}$$

where Ω is the atomic volume. This result is simply a consequence of the fact that for a homogeneous and isotropic dilation of the crystal lattice both the linear dimensions of the Brillouin zone of the reciprocal lattice and the radius k_F of the Fermi sphere scale like $\Omega^{-1/3}$. In this model the shape of the energy bands does not depend on the atomic volume. The density of states $n(E_F)$ is however proportional to $\Omega^{2/3}$ and

$$\frac{d\ln n(E_F)}{d\ln\Omega}=\frac{2}{3} \tag{21}$$

In the *pure d-band* model the width of the d-band varies as $\Omega^{-5/3}$ [69h2]. In order to conserve the number of electrons the Fermi energy scales exactly like the dispersion curves $E(k)$, i.e.

$$\frac{d\ln(E_F-d_0)}{d\ln\Omega}=-\frac{5}{3} \tag{22}$$

where d_0 is the energy of the centre of the d-band. The volume dependence of any cross-sectional area of the Fermi surface is then determined only by the linear expansion of the Brillouin zone and

$$\frac{d\ln A}{d\ln\Omega}=-\frac{2}{3} \tag{23}$$

as in the nearly-free-electron model. Since the total number of states in the band is independent of the atomic volume, the density of states increases as $\Omega^{5/3}$ and

$$\frac{d\ln n(E_F)}{d\ln\Omega}=\frac{5}{3} \tag{24}$$

In real metals significant departures from the predictions of these two simple models are expected as a result of the deformation of the energy bands near Bragg planes and of the simultaneous presence of s-, p- and d-bands (and f-bands) in transition metals (and rare-earth metals).